We are IntechOpen,
the world's leading publisher of
Open Access books
Built by scientists, for scientists

4,800
Open access books available

122,000
International authors and editors

135M
Downloads

Our authors are among the

154
Countries delivered to

TOP 1%
most cited scientists

12.2%
Contributors from top 500 universities

CLARIVATE ANALYTICS
BOOK CITATION INDEX
INDEXED

WEB OF SCIENCE™

Selection of our books indexed in the Book Citation Index
in Web of Science™ Core Collection (BKCI)

Interested in publishing with us?
Contact book.department@intechopen.com

Numbers displayed above are based on latest data collected.
For more information visit www.intechopen.com

Purification of Rare Earth Amide Salts by Hydrometallurgy and Electrodeposition of Rare Earth Metals Using Ionic Liquids

Masahiko Matsumiya

Abstract

This paper reports a novel bench-scale hydrometallurgical procedure and electrodeposition using triethyl-pentyl-phosphonium bis(trifluoromethyl-sulfonyl)amide ($[P_{2225}][TFSA]$) ionic liquids (ILs) for the recovery of rare earth (RE) metals from spent Nd-Fe-B magnets. The hydrometallurgical treatments were carried out at bench scale to produce RE amide salts of high purity. In the leaching process employing 1.7 kg of oxidized Nd-Fe-B fine powder and 14.2 L of an acid medium of 1,1,1-trifluoro-*N*-[(trifluoromethyl)sulfonyl]methanesulfonamide (H[TFSA]), selective leaching of RE ions (85.7±5.8% Nd) was performed at bench scale. Then, Fe (<99.9%) was successfully separated from RE ions in the deironization process. The total amount of the recovered amide salts through the evaporation treatment using a spray dryer was 3.57 kg. From the CV/EQCM measurements for Nd(III) at 373 K, a clear cathodic peak with the mass increased, and the $\eta\rho$ decreased was observed at −2.79 V. Considering our previous investigations, the reduction of Nd(III)/Nd(0) was indicated as $[Nd^{(III)}(TFSA)_5]^{2-} + 3e^- \rightarrow Nd(0) + 5[TFSA]^-$. In addition, the M_{app} value in the range of −2.49 V ~ −2.94 V was 46.8 g mol^{-1}, which was close to the theoretical value for the electrodeposition reaction of Nd(III)/Nd(0), 48.1 g mol^{-1}. Moreover, the electrodeposition of Nd(0) was carried out under the condition of −3.20 V versus Fc/Fc$^+$ at 373 K. The electrodeposits were identified with the metallic Nd in the middle layer investigated by X-ray diffraction and X-ray photoelectron spectroscopy. Finally, we demonstrated that the novel recovery process consisted of hydrometallurgy and electrodeposition using ILs was effective by calculating material flow.

Keywords: electrodeposition, hydrometallurgy, ionic liquids, neodymium metal

1. Introduction

Rare earth (RE) elements are currently regarded to be the most critical elements necessary for sustainable applications, and their RE groups play an important role in the development of future high-tech industries. Significant price fluctuations and high demand have raised their potential recovery from end-of-life products [1]. It is important to recover them from urban mining and secondary products containing permanent magnets.

Hydrometallurgical treatment is widely applied as an effective method for extracting RE components from primary sources and is potential in reclaiming these elements [2]. As listed in **Table 1**, the various techniques effective for the recovery of RE elements, such as chemical vapor transport [3], solvent extraction [4], electrolytic method [5], and hydrometallurgical processes [6, 7], have been listed, although a number of recovery methods for RE elements on the laboratory scale have not been so widespread. There was almost no information about the plants and processing paths. From the above situation, this study focused on a bench-scale hydrometallurgy to separate and recover RE components from spent Nd-Fe-B magnet. The preliminary research in our procedure is reported in the previous publications [8, 9].

Methods	Remarks	Reference
Chemical vapor transport	59% Nd and 68% Dy were recovered from scrap of RE intermetallic materials.	[3]
Solvent extraction and liquid-membrane transport	The selective permeation of Nd and Dy by IL based supported liquid-membrane using *N,N*-dioctyldiglycolamic acid.	[4]
Electrolysis	Polarization on Pt electrode led to recover Nd and Dy metals in fused Na_2SO_4 from Nd and Dy oxides	[5]
Electrochemical process	Mass ratio between Nd and Dy was indicated as 121 from RE-Ni alloys	[6]
Hydrometallurgical process	The recovery efficiencies were indicated as 69.7% Nd and 51% Dy from magnetic waste sludge	[7]

Table 1. Various recovery techniques for rare earths.

Pyrometallurgical treatment using high-temperature molten salts (HTMSs) is generally known as a conventional method for the recovery of RE metals. However, the HTMSs such as fluorides [10, 11] consumes a large amount of thermal energy owing to the high melting points of molten salts; thus, the recovery method of RE metals from HTMS baths is inappropriate as a next-generation technique. From the standpoint of saving energy, the development of a recovery process for RE metals with reduced energy consumption is hopeful in the near future. For this purpose, we have proposed an electrowinning-recovery method of the REs using ILs, which have unique physicochemical properties, such as high ionic conductivity, a wide electrochem-

ical window, low vapor pressure, and incombustibility [12]. The electrochemical behaviors and the electrodepositions of RE metals such as La, Sm, Eu, and Yb in ILs are reported [13, 14]. We have already demonstrated the electrochemical behaviors and the electrodepositions of Nd [15–18] and Dy metals [19, 20] using hydrophobic ILs, such as triethyl-pentyl-phosphonium bis(trifluoromethyl-sulfonyl) amide [P$_{2225}$][TFSA] and 2-hydroxyethyl-trimethyl-ammonium bis(trifluoromethyl-sulfonyl) amide [N$_{1112}$OH][TFSA]. In addition, we have developed the wet separation processes such as the solvent extraction using the hydrophobic ILs [21–23] and the precipitation separation [8, 9]. The wet separation process was combined with the electrodeposition for the recovery of the Nd and Dy metals from the practical wastes of Nd-Fe-B magnets.

For the purpose of the analysis of reduction behavior of Nd(III) in ILs, in situ investigation using an electrochemical quartz crystal microbalance (EQCM) was conducted in this study. The EQCM technique is based on the piezoelectric properties of a quartz crystal and can detect a nano-level mass change in a quartz crystal electrode during electrochemical experiments from the resonance frequency of the quartz [24]. Although a conventional oscillator technique, namely self-excited or active technique EQCM, was inoperative in some ILs due to their high viscosity, the possibility of applying EQCM measurements with the use of separately excited or passive technique in highly viscous fluids including ILs was recently demonstrated and the cases of successful application have been reported [25–30]. On the EQCM measurement, the resonance resistance can also be measured and reflects a product of the viscosity and the density of the media near the quartz crystal electrode [28] and the viscoelasticity of the electrodeposits [26, 27, 31, 32]. Thus, the change in the mass and the viscoelasticity of the electrodeposits on the electrode and the product of the viscosity and the density of the electrolyte near the electrode, relating to the concentration of a soluble species particularly in the case of ILs [25, 26] and corresponding to the electrochemical behavior, can simultaneously be observed by using the EQCM measurements, and very useful information for the specific examination of the electrode reaction can be acquired.

In this study as a new attempt, the electrochemical behavior of Nd(III) in ILs was analyzed by EQCM measurement at elevated temperatures because it is desirable to decrease the overpotential of the electrodeposition and to increase the diffusion rate of the metallic species by lowering the viscosity by means of elevating the temperature. There were a few reports about the theoretical equations: the Sauerbrey equation [24] and Kanazawa-Gordon [33]. However, these equations were not applied at elevated temperatures [25, 34]; therefore, we have demonstrated that the applicability of EQCM method in a medium temperature range around 373 K was revealed in the previous study [35]. In addition, we discuss the electroreduction behavior of Nd(III) in ILs on the potentiostatic condition in this study.

Considering the fundamental electrochemical investigations, the electrodeposition on the condition of constant potential was carried out on a relatively large scale. The Nd metal recovered by electrodeposition is applicable in the production of new Nd-Fe-B magnets because Nd metal of high purity is obtained by polishing the oxide layer after electrodeposition using ILs. Finally, we demonstrated the effectiveness of hydrometallurgy and electrodeposition process through the material flow.

2. Experimental

2.1. Pretreatment process

The spent Nd-Fe-B magnets were recovered from voice coil motors (VCMs) that were heated in an electric furnace at 623 K for 3 h for the demagnetization treatment. After demagnetization, the magnetic flux density was measured using a digital TESLA meter. The residual magnetic force field of this sample was almost zero, and the percentage of demagnetization was >99.9%. Then, the Ni-Cu-Ni triple layer on the Nd-Fe-B sample was removed by a grinding machine. After the stripping of the layer, fragments of Nd-Fe-B sample were pulverized using a stamp mill. The fine powders obtained were sieved to less than 150 μm and heated at 90 K h^{-1} to 1133 K, which was kept for 3 h in an electric furnace in order to oxidize the Nd-Fe-B components. After the roasting process, these fine powders were reground again by the automatic grinder. The surface area and the particle size (D50) of oxidized Nd-Fe-B sample measured by the Brunauer-Emmett-Teller (BET) method were 0.630 m^2 g^{-1} and 59.43 μm, respectively.

2.2. Bench-scale leaching

The fine powders of oxidized Nd-Fe-B sample (1.7 kg) were leached in 14.2 L of a 1.0 M aqueous solution of 1,1,1-trifluoro-N-[(trifluoromethyl)sulfonyl]methanesulfonamide (HN(SO$_2$CF$_3$)$_2$, H[TFSA]). The leaching solution was heated at 323 K, stirring at 500 rpm. The leaching behavior was researched from the potential (E)-pH diagram for Fe-H$_2$O and Nd-H$_2$O systems. Therefore, the oxidation-reduction potential (ORP) and pH in the leaching solution were measured by a high-precision digital meter (MM-60R, DKK-TOA Corp.). The quantification of Fe^{2+} was available for the complexation of [Fe(phen)$_3$]$^{2+}$ using 1,10-phenanthroline. The concentration of Fe^{2+} was measured by an ultraviolet-visible-near-infrared (UV-Vis-NIR) spectrometer (Perkin Elmer, Lambda750) at 508 nm [36, 37]. The concentration of Fe^{3+} was calculated from the total amount of Fe^{2+} and Fe^{3+} ions obtained from inductively coupled plasma atomic emission spectroscopy (ICP-AES) analysis (ICPE-9000, Shimadzu Co.). All of the precise concentrations for metallic species were quantitatively determined from ICP-AES analysis.

2.3. Bench-scale deironization and preparation of RE salts

Dried oxygen gas was introduced into the leaching solution with a flow rate of 5.0 L min^{-1} after the leaching process. The oxidizing agent for Fe^{2+} was effective in the leaching solution at pH > 3.2. Some kinds of alkali metal hydroxides [8, 9] were acted as precipitation agents in the previous study, and the perfect removal of the iron components was successfully carried out at laboratory scale. The deironization treatment without precipitation agents is important as a further development, because the additive materials contaminated the final RE salts. Considering the leaching process, reuse of the oxidized Nd-Fe-B powder as a precipitation agent is desirable, because RE$_2$O$_3$ in the oxidized Nd-Fe-B sample was selectively leached in the H[TFSA] solution. The oxidized Nd-Fe-B fine powder was also available for sediment formation of [Fe(OH)$_x$]$^{3-x}$ precipitates in this study. A small amount of the oxide Nd-Fe-B powder was introduced carefully into leaching solution while the alternation in pH was

measured. The best terminal point of the precipitation reaction for $[Fe(OH)_x]^{3-x}$ was found to be pH = 4.92–4.93 because no iron component was detected in the leaching solution. It was important to develop a rapid solid-liquid separation technique because $[Fe(OH)_x]^{3-x}$ precipitates are colloidal and the separation from colloidal precipitates is very difficult. Therefore, hematite (α-Fe$_2$O$_3$) containing oxidized Nd-Fe-B sample was applied as a seed crystal in the formation of $[Fe(OH)_x]^{3-x}$ precipitates. The formation of $[Fe(OH)_x]^{3-x}$ precipitates with a large particle size greatly contributed to the filtration in solid-liquid separation. Finally, the $[Fe(OH)_x]^{3-x}$ precipitates were completely removed from the leaching solution.

After the deironization treatment, a turquoise filtrate was obtained; the color of the solution was based on the RE components. The evaporation treatment of the filtrate was carried out by a spray dryer (SD-1000, EYELA Co., Ltd.). In the operation of the spray dryer, the inlet temperature was maintained at 473 ± 1.6 K and dried nitrogen gas was introduced through the evaporation part at 105 ± 5.0 kPa. Then, the H[TFSA] filtrate was introduced using a roller pump at 150 mL h^{-1}. In order to recover the dried M(TFSA)$_n$ salts, the recovery part was heated at 413 ± 1.5 K with a heating mantle. The amount of M(TFSA)$_n$ salts for one batch and the total amount of M(TFSA)$_n$ salts were >300 g and 3.57 kg, respectively. The amount of metallic components in the M(TFSA)$_n$ salts was measured by ICP-AES analysis.

2.4. Electrochemical analysis

The resistance of a quartz oscillator and resonance frequency were observed using an EQCM system, (Seiko EG&G, QCA922) applying AT-cut platinum-coated [9 MHz, φ = 5.0 mm, Seiko EG&G, QA-A9M-PT(P)] with a well-type cell (Seiko EG&G, QA-CL4PK) as shown in **Figure 1**. The employed O-rings (Seiko EG&G, P-S75B) had a high resistance for heat and low expansibility. The temperature of the EQCM system was elevated using a heating mantle controlled by a thermostat with a proportional-integral-derivative (PID) controller. The temperature was slowly increased at a rate of 1.0–1.5 K min^{-1} to prevent the strain occurring in the crystal structure of the quartz. The bath temperature was measured using a K-type thermocouple (φ = 1.6 mm). The cell covered with the heating mantle was connected to the EQCM system with an extension cord (Seiko EG&G, QCA922-10-EX10). In terms of the functionality of EQCM technique at elevated temperatures, the relationship between the viscosity and the density of Nd(III) samples, $\eta\rho$ values, the shifts of the resonance frequency, and the resistance before and after contacting the samples with the quartz have been already revealed in the previous study [35].

The voltammetric measurements were carried out using an electrochemical analyzer (ALS-440A, BAS Inc.,) with the EQCM system employing the Pt-coated quartz oscillator as a working electrode. Two Pt wires with 0.5 mm inside diameter were used as a counter and a quasi-reference electrode (QRE). The counter electrode was surrounded by a Vycor glass filter at the bottom in order to prevent the diffusion of decomposition components from the anode into the electrolyte. The Pt QRE showed a high stability and a good reproducibility of the potential at elevated temperatures. The potential was compensated for the IL standard using a ferrocene (Fc)/ferrocenium (Fc$^+$) redox couple. Before all the electrochemical measurements, the dissolved oxygen was removed from the electrolytes by bubbling Ar gas for 30 min, and
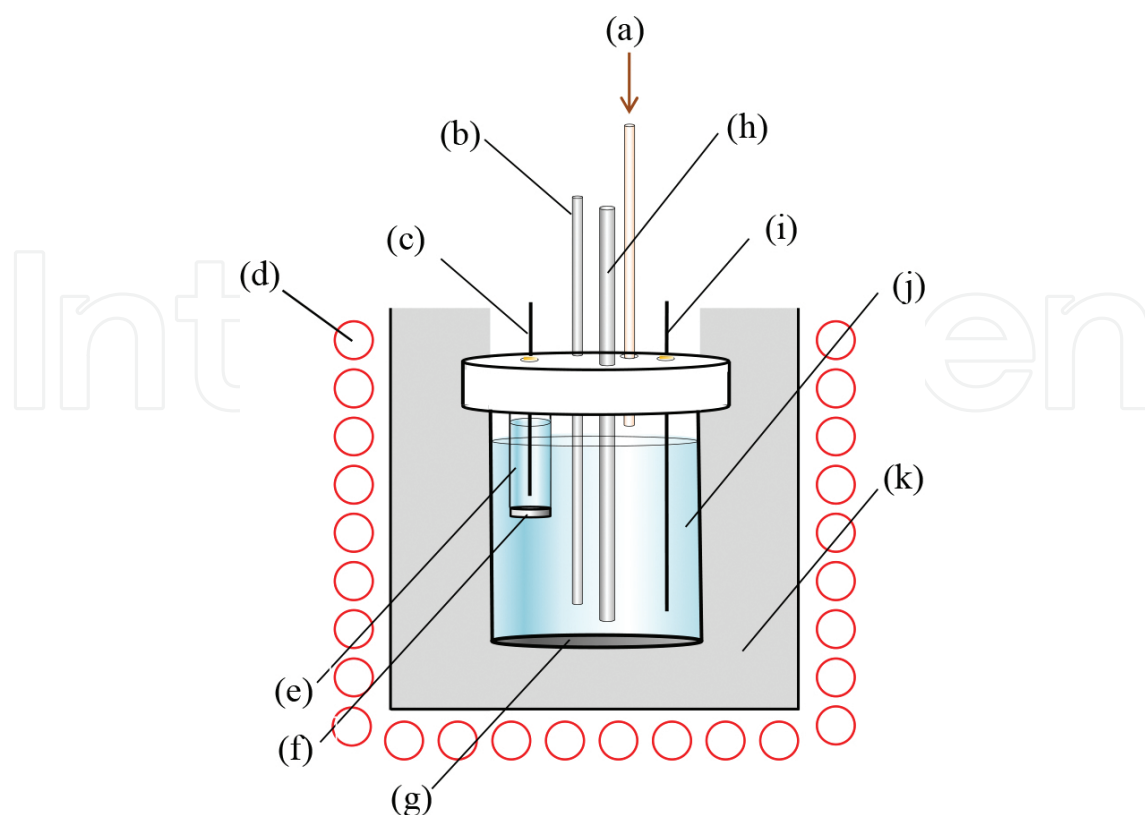
Figure 1. The schematic illustration of EQCM cell with separate system: (a) Ar flow, (b) K-type thermocouple-1 (for recording by a data logger), (c) Pt wire (counter electrode), (d) heating mantle, (e) separated electrolyte, (f) Vycor glass, (g) quartz oscillator coated with Pt (working electrode), (h) K-type thermocouple-2 (for controlling temperature by PID), (i) Pt wire (quasi-reference electrode), (j) main electrolyte, (k) heat insulator.

the measurements were conducted under flowing Ar gas in the cell with a rate of 20 ml min^{-1}. Cyclic voltammetry (CV) of 0.01 M Fc in [P_{2225}][TFSA] was carried out at 298 K with a sweep rate of 1.0 mV s^{-1} after *iR* compensation (RC constant: 977.3) in order to confirm EQCM behavior while there was an outer-sphere electron-transfer reaction of Fc/Fc$^+$. The electrochemical behavior of Nd(III) in [P_{2225}][TFSA] was investigated by CV measurements of 0.05 M Nd(III) in [P_{2225}][TFSA] at 373 K with a sweep rate of 2.0 mV s^{-1}. For the analysis of the electrodeposition behavior of Nd(0) from Nd(III) in [P_{2225}][TFSA], the controlled potential electrolysis (CPE) under −3.20 V vs. Fc/Fc$^+$ was performed at 373 K using 0.05 and 0.10 M Nd(III) in [P_{2225}][TFSA] as electrolytes.

2.5. Electrodeposition

A schematic illustration of the electrodeposition cell is shown in **Figure 2**. In the electrodeposition with the three-electrode system, a copper substrate with a surface area of 2.0×10^{-2} m^2 and a platinum were employed as the working electrode and quasi-reference electrode, respectively. Fe rod was employed as a counter electrode and was surrounded with a glass tube via a Vycor glass filter at the bottom to prevent the diffusion of dissolved [Fe(TFSA)$_3$]$^-$ complexes from the anode into the electrolyte. The electrolytic bath was stirred at 500 rpm, because the current during electrodeposition decreased immediately to the limiting current

when the bath was not stirred. The overpotential was constant at −3.20 V versus Fc/Fc⁺ at 373 K during potentiostatic electrodeposition in a glovebox. After electrodeposition, the electrodeposits were leached into a super-dehydrated acetone (>99.5%, Wako Pure Chemical Industries, Ltd., water content <10 ppm) in a glovebox to remove the electrolyte thoroughly. The surface morphology of the electrodeposits was observed by scanning electron microscopy (SEM) and the composition of the electrodeposits was analyzed by energy dispersive X-ray analysis (EDX) (JSM-6510LA, JED-2300, JEOL, Ltd.). The metallic state and the crystallinity of the electrodeposits were evaluated by X-ray photoelectron spectroscopy (XPS) (Quantera SXM, ULVAC-PHI, Inc) and X-ray diffraction (XRD) (RINT-2500, Rigaku Co.), respectively.
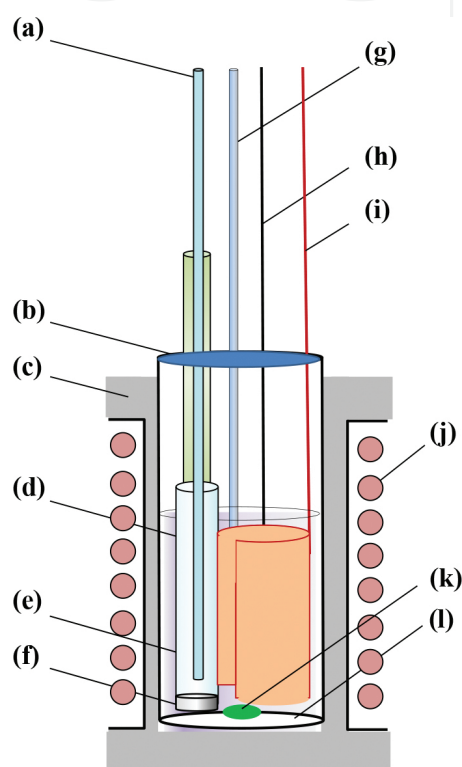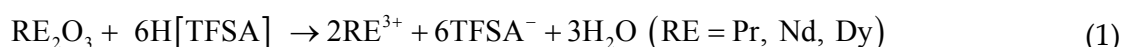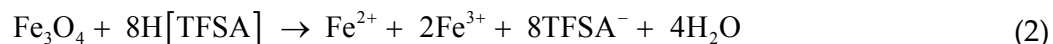

Figure 2. The schematic illustration of the electrodeposition cell with three-electrode system, (a) Fe rod (anode), (b) Teflon cap, (c) heat insulator, (d) soda-lime glass tube, (e) $[P_{2225}][TFSA]$, (f) Vycor glass filter, (g) K-type thermocouple, (h) Pt wire (Q.R.E.), (i) Cu substrate (cathode), (j) heating mantle, (k) stirrer, and (l) $[P_{2225}][TFSA]$ including $M(TFSA)_n$ or $Nd(TFSA)_3$.

3. Results and discussion

3.1. Leaching behavior at bench scale

The leaching reactions of the oxidized Nd-Fe-B sample were represented as follows:

$$RE_2O_3 + 6H[TFSA] \rightarrow 2RE^{3+} + 6TFSA^- + 3H_2O \ (RE = Pr, \ Nd, \ Dy) \tag{1}$$

$$Fe_3O_4 + 8H[TFSA] \rightarrow Fe^{2+} + 2Fe^{3+} + 8TFSA^- + 4H_2O \tag{2}$$

The leaching behavior in H[TFSA] solution using the oxidized Nd-Fe-B fine powder as a precipitation agent is shown in **Figure 3**. The leaching percentage of Nd and Fe for 66h in the H[TFSA] solution were 85.7±5.8% and 5.8±0.1%, respectively. A drastic increase in the pH value was observed at the initial stage of the leaching process, which indicates that leaching reaction Eq. (1) mainly occurred in this system. The leaching behavior accounted for the potential (E)-pH diagrams of Fe-H_2O and Nd-H_2O systems as shown in **Figure 4**. The actual measurement data in the bench scale is also plotted in the potential (E)-pH diagram. From the E-pH diagram, at E = ~0.75 and pH < 1.0, the most stable states of Fe and Nd components were found to be solid Fe_2O_3 and Nd^{3+} ion, respectively. This result indicated that the selective leaching of Nd^{3+} (leaching percentage > 90%) was carried out at bench scale.
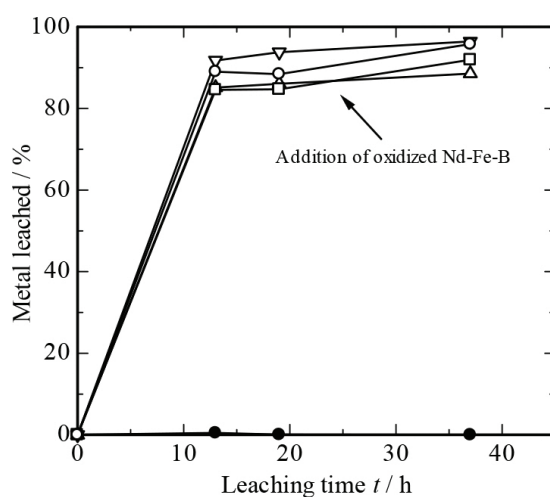

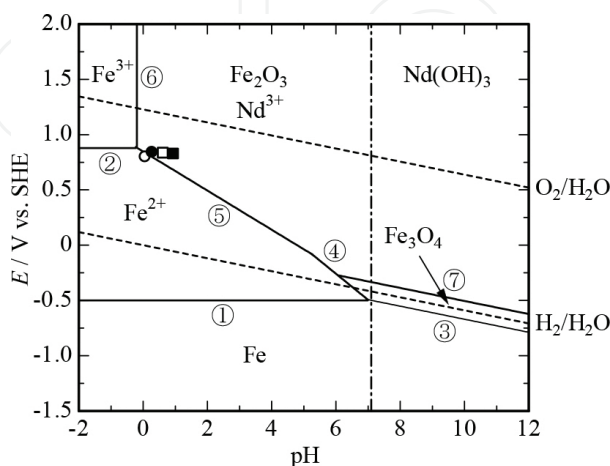**Figure 3.** The leaching behavior of each metallic component in H[TFSA] solution at bench scale.

Figure 4. Potential(E)-pH diagram of Fe-H_2O and Nd-H_2O systems. Leaching time ○:3 h, ●:15 h, □:18 h, ■:21 h.

3.2. Deironization and purification of RE amide salts at bench scale

The effective treatment for deironization is precipitation separation through the oxidation from Fe^{2+} to Fe^{3+} by oxygen bubbling, because $[Fe(OH)_x]^{3-x}$ precipitates are formed under acidic pH conditions [8, 9]. The precipitation reaction using the oxidized Nd-Fe-B sample was expressed as follows:

$$2Fe^{3+} + RE_2O_3 + 3H_2O \rightarrow 2\left[Fe(OH)_x\right]^{3-x} + 2RE^{3+}\left(RE = Pr, Nd, Dy\right) \qquad (3)$$
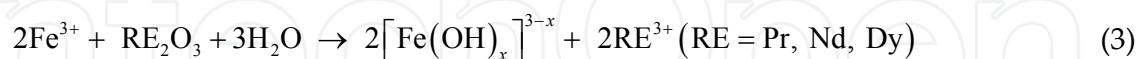
$[Fe(OH)_x]^{3-x}$ is generally a colloidal precipitate, and it is very difficult to separate from the H[TFSA] solution. Therefore, we applied a seed crystal method, and hematite (α-Fe_2O_3) in oxidized Nd-Fe-B sample was employed as a seed crystal for the formation of $[Fe(OH)_x]^{3-x}$ precipitates. The precipitate with a large particle size greatly facilitated the filtration in the solid-liquid separation treatment. From the ICP-AES analysis, the separation percentage of Fe component was confirmed to be >99.9%. This result allowed us to conclude that the oxidized Nd-Fe-B sample was applicable for perfect removal of iron component as a seed crystal.

After the solid-liquid separation, the evaporation treatment of filtrate was performed using an improved spray dryer to effectively recover dried $M(TFSA)_n$ (M = Pr, Nd, Dy, B, Al, K, and trace elements) salts. The refining conditions of the H[TFSA] solution for the oxidized Nd-Fe-B sample are listed in **Table 2**. The total amount of recovered $M(TFSA)_n$ and the average

Run no.	Flow rate /mL min^{-1}	Blower flow rate/m^3 min^{-1}	Volume of H[TFSA] aq./mL	Amount of $M(TFSA)_n$/g	Recovery Yield/%
1	2.5	0.35–0.50	150	35.10	82.4
2	2.5	0.35–0.50	300	73.25	84.7
3	2.5	0.35–0.50	450	110.81	88.1
4	2.7	0.35–0.50	600	154.13	89.8
5	2.7	0.15–0.35	750	201.97	91.8
6	2.7	0.15–0.35	1050	273.85	91.2
7	2.9	0.15–0.35	1200	314.59	91.6
8	2.9	0.15–0.35	1200	320.62	93.7
9	2.9	0.15–0.35	1200	321.73	93.5
10	2.9	0.15–0.35	1200	325.64	94.4
11	2.9	0.15–0.35	1200	329.89	95.3
12	2.9	0.15–0.35	1200	328.74	94.6
13	2.9	0.15–0.35	1200	387.83	95.8
14	2.9	0.15–0.35	1200	393.32	96.8
				Total: 3571.5 g	Ave.: 91.7%

Table 2. The refining condition of leaching solution by spray dryer.

recovery yield were 3571.5 g and 91.7%, respectively. The obtained $M(TFSA)_n$ salt was a fine pale purple powder, and the water content in the $M(TFSA)_n$ salt was less than 10 ppm. The composition of the recovered $M(TFSA)_n$ salts is tabulated in **Table 3**. The stoichiometric number of $M(TFSA)_n$ and average molecular weight were 3.00 and 943.68, respectively. In addition, the average RE component in $M(TFSA)_n$ was 96.81%. This series of results allowed us to conclude that the separation factor of Fe in the deironization treatment was >99.9% and the recovery yield of $M(TFSA)_n$ salts was 82.4–96.8% using a spray dryer at bench scale.

Run no.	Pr	Nd	Dy	RE[*]	Fe	B	Molecular weight of $M(TFSA)_n$	n [**]
1	20.81	72.87	2.48	96.16	0.00	3.84	938.15	3.00
2	20.76	73.55	2.47	96.78	0.00	3.22	943.46	3.00
3	19.80	74.96	2.06	96.82	0.00	3.18	943.77	3.00
4	19.39	74.78	2.46	96.63	0.00	3.37	942.11	3.00
5	19.83	74.58	2.46	96.87	0.00	3.13	944.26	3.00
6	19.80	74.77	2.40	96.96	0.00	3.04	944.26	3.00
7	19.53	74.85	2.53	96.91	0.00	3.09	944.71	3.00
8	19.86	74.87	2.05	96.78	0.00	3.22	943.42	3.00
9	20.01	74.80	2.00	96.82	0.00	3.18	943.78	3.00
10	20.07	74.84	1.99	96.90	0.00	3.10	944.52	3.00
11	21.05	73.93	1.97	96.95	0.00	3.05	944.98	3.00
12	20.10	74.77	2.13	96.99	0.00	3.01	945.40	3.00
13	19.75	74.99	2.16	96.89	0.00	3.11	944.45	3.00
14	20.01	74.73	2.12	96.87	0.00	3.13	944.23	3.00
Ave.	20.06	74.52	2.23	96.81	0.00	3.19	943.68	3.00

[*]RE indicates the summation of the composition for Pr, Nd, and Dy.
[**]n indicates the stoichiometric number of $M(TFSA)_n$ salts.

Table 3. The composition (wt.%) of recovered $M(TFSA)_n$ salts on the condition of **Table 1**.

3.3. Theory

A frequency shift (Δf) observed on the EQCM analyzer includes effects relating to the mass change (Δm) in the quartz crystal electrode (Δf_m) and the viscosity (η) and the density (ρ) of the liquid adjacent to the quartz ($\Delta f_{\eta\rho}$).

$$\Delta f = \Delta f_m + \Delta f_{\eta\rho} \tag{4}$$

The relationship between Δf_m and Δm is expressed by the Sauerbrey equation [24].

$$\Delta f_m = \frac{2f_0^2 \Delta m}{A\left(\mu_q \rho_q\right)^{1/2}}$$ (5)

where f_0 is the fundamental resonance frequency, A is the surface area of the electrode (0.196 cm^2), μ_q is the shear modulus of quartz (2.95×10^{10} kg m^{-1} s^{-2} at 298 K), and ρ_q is the density of quartz (2.65×10^3 kg m^{-3} at 298 K). On the other hand, $\Delta f_{\eta\rho}$ is proportional to the square root of the product of the liquid viscosity and density, $(\eta\rho)^{1/2}$ demonstrated by Kanazawa-Gordon [33].

$$\Delta f_{\eta\rho} = -f_0^{\frac{3}{2}}\left(\frac{\eta\rho}{\pi\mu_q\rho_q}\right)$$ (6)

Although a frequency shift by the aqueous solution contacting the quartz is small, in the case of employing ILs as the electrolyte, it is necessary to consider the influence of $\Delta f_{\eta\rho}$ due to the exceedingly high viscosity of ILs. In the EQCM measurements, the resonance resistance (R) can simultaneously be measured, and $(\eta\rho)^{1/2}$ is also estimated from R value [38].

$$R = \frac{A\left(2\pi f_0 \eta\rho\right)^{1/2}}{k^2}$$ (7)

where k is an electromechanical coupling factor and often used when the electrical model of the quartz crystal oscillator is converted to a mechanical model. The k value was estimated from the shifts in the resonance frequency and the resistances before and after the liquid sample came into contact with the quartz according to Eqs. (6) and (7), respectively, for each measurement in this study. Δf_m is isolated from the total shift of frequency (Δf) by using Eqs. (4), (6), and (7). In addition, the apparent molar mass, M_{app}, of the electrodeposited species can be calculated by using Δm estimated from Δf_m, the electrical charge Q passed during electrodeposition, and the Faraday constant F.

$$M_{app} = \frac{F\Delta m}{\Delta Q}$$ (8)

The theoretical value of M_{app} based on the reduction reaction of Nd(III) + 3e$^-$ → Nd(0) was 48.1 g mol^{-1}. The theoretical equations of the EQCM measurements related to the frequency response are based on the analysis of an admittance spectrum of the quartz crystal near its resonance frequency [39]. The responses of the resonance frequency and the resistance to $(\eta\rho)^{1/2}$ of the adjacent liquid to the quartz crystal are derived from the solutions of the equation, describing the steady-state shear waves in the AT-cut quartz oscillator under the condition that the transverse velocity of the surface of the quartz oscillator is identical with that of the adjacent liquid and that the force exerted by the liquid on the quartz is equal and opposite to the force

exerted by the quartz on the liquid [33, 38]. Strictly speaking, the estimation of Δm from Δf_m by Eq. (4) is valid for thin and rigid films coated on the quartz. Moreover, $\Delta f_{\eta\rho}$ and R reflect not only the viscosity and the density of contacting liquid with the quartz but also the roughness, the viscoelastic properties, and the films [31, 32]. By considering these parameters in combination, it is possible to discuss detailed states on the surface of the quartz electrode accompanied by the electrochemical behaviors.

3.4. Electrochemical analysis

For the investigation of the reduction behavior for Nd(III) in [P$_{2225}$][TFSA], cyclic voltammetry with EQCM measurements (CV/EQCM) were carried out at elevated temperatures. The EQCM behavior was confirmed in advance by CV/EQCM at 298 K measuring Fc/Fc$^+$ redox couple in [P$_{2225}$][TFSA]. The potential difference, ΔE_p, between the anode and cathode peak was 67 mV after iR compensation. The ΔE_p value was close to the theoretical value; 59 mV in a reversible and one-electron reaction at 298 K and thus the observation of the electrochemical behavior was confirmed with high precision. Moreover, there were no significant alternations for the mass and $\eta\rho$ values in this reversible reaction. The results indicated that no changes of Δm and $\Delta\eta\rho$ were detected during the outer-sphere electron-transfer reaction and consistent with the Ref. [26].

The CV/EQCM results for Nd(III) in [P$_{2225}$][TFSA] at 373 K were shown in **Figure 5**. A clear cathodic peak with the mass increased and the $\eta\rho$ decreased was observed at −2.79 V. Considering our previous investigations [15–18], the reduction of Nd(III)/Nd(0) was indicated as follows:

$$[\text{Nd}^{(\text{III})}(\text{TFSA})_5]^{2-} + 3\text{e}^- \rightarrow \text{Nd}(0) + 5[\text{TFSA}]^- \tag{9}$$

The M_{app} value in the range of −2.49 V ~ −2.94 V calculated from the mass change was 46.8 g mol^{-1}, which was close to the theoretical value for the electrodeposition reaction of Nd(III)/Nd(0), 48.1 g mol^{-1}. Moreover, the observed decrease of the $\eta\rho$ value indicated that the concentration of Nd(III) near the electrode was locally decreased by consuming Nd(III) in the electrodeposition reduction of Nd(III)/Nd(0). This is based on the $\eta\rho$ change in the IL system that largely depends on the concentration of the metal ion. Therefore, these results are an evidence for the electrodeposition reaction of Nd(III)/Nd(0). At a more negative potential than −2.79 V, the mass and $\eta\rho$ increased with the comparatively low values of M_{app} for 0.05 M Nd(III) in [P$_{2225}$][TFSA]. This behavior indicated that the cathodic decomposition products from IL were generated on the electrode surface. A part of side chain of [P$_{2225}$]$^+$ would be decomposed on the cathode considering the M_{app} value estimated in this potential range (−2.96 V ~ −3.30 V). In addition, in the range of 0 ~ −2.0 V the mass unexpectedly increased during slight current and no change in the $\eta\rho$ value for 0.05 M Nd(III) in [P$_{2225}$][TFSA]. There was no observation of mass increase in the EQCM analysis for neat [P$_{2225}$][TFSA] in this potential. Therefore, it was deduced that the reaction would be the formation of divalent species; Nd(II) [Nd(III) + e$^-$ → Nd(II)]. The related disproportionation reaction [2Nd(III) + Nd(0) → 3Nd(II)] would occur in the IL system.
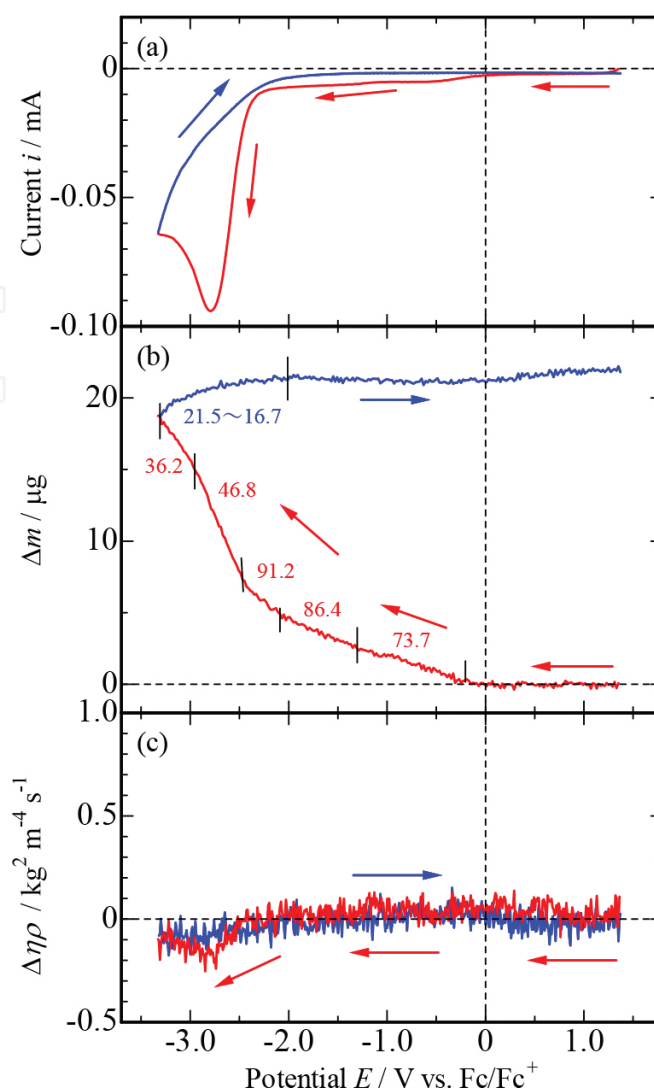
Figure 5. CV/EQCM analysis for 0.05 M Nd(III) in [P$_{2225}$][TFSA] at 373 K with 2.0 mV s^{-1}; (a) voltammogram, (b) the mass change, and (c) the change in $\eta\rho$ values.

The controlled potential electrolysis with EQCM measurements (CPE/EQCM) at −3.20 V was conducted with 0.05 and 0.10 M Nd(III) in [P$_{2225}$][TFSA] at 373 K. The parameters of Δm and $\Delta\eta\rho$ were plotted as a function of the charge density Q_d passed during CPE as shown in **Figure 6**. The calculated values of M_{app} in 0.05 and 0.10 M Nd(III) at the initial stage of CPE/EQCM analysis were 49.1 and 49.6 g mol^{-1}, respectively, which were close to the theoretical value when the reduction of Nd(III)/Nd(0) occurred, 48.1 g mol^{-1}, so that the electrodeposition of Nd(0) metal was also proved from the CPE/EQCM analysis. The total values of M_{app} in 0.10 M solution, 18.4 ~ 29.8 g mol^{-1}, were larger than those in 0.05 M solution, 7.7 ~ 18.6 g mol^{-1}. These results indicated that the competition reaction for Nd(III)/Nd(0) reduction and IL decomposition would occur and depend on the Nd(III) concentration. The value of $\eta\rho$ after 0.45 C cm^{-2} increased and the IL decomposition was also deduced from this result because the $\eta\rho$ change implied that the quantity of the soluble species increase near the electrode and/or the viscoelastic film might be formed on the electrode surface [27, 31, 32, 40] by the IL decomposition.
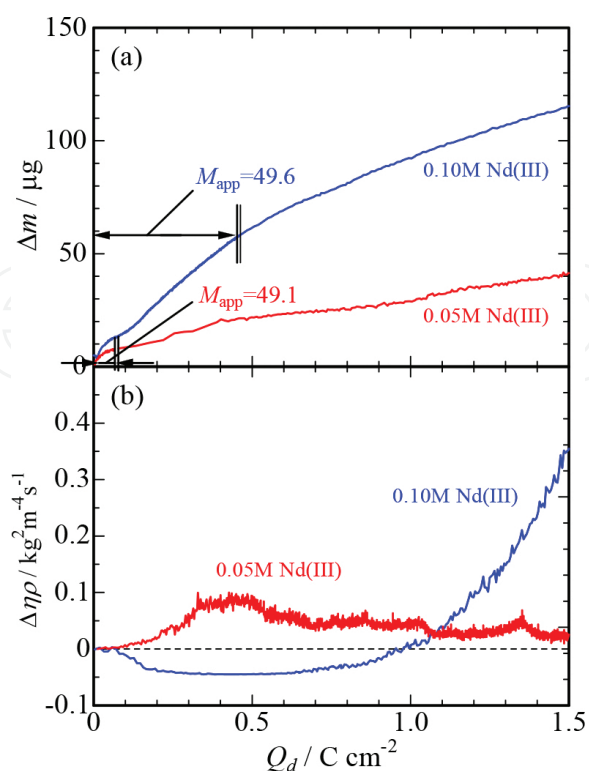
Figure 6. CPE/EQCM analysis for 0.05 and 0.10 M Nd(III) in [P_{2225}][TFSA] induced on ⁻3.20 V at 373 K; (a) the mass change and (b) the change in $\eta\rho$ values.

Run no.	Overpotential, η/V vs. Fc/Fc⁺	Transported charge, Q/C	Weight change, Δw/g	Current efficiency, ε/%
1	−3.20	6054.6	Anode:−1.694	Anode:96.7
			Cathode:+2.184	Cathode:72.4
2	−3.20	6634.8	Anode:−1.794	Anode:93.4
			Cathode:+2.541	Cathode:76.9
3	−3.20	7618.2	Anode:−2.094	Anode:95.0
			Cathode:+2.832	Cathode:74.6

Table 4. The potentiostatic electrodeposition condition using [P_{2225}][TFSA] including M(TFSA)₃ at 373 K.

Run no.	Composition/wt.%								
	C	N	O	F	P	S	Fe	Cu	Nd
1	5.52	0.84	12.38	0.46	0.31	0.96	0.02	15.82	63.69
2	3.62	0.43	9.62	0.32	0.18	0.68	0.00	13.64	71.51
3	4.82	0.68	10.23	0.36	0.23	0.82	0.00	12.46	70.40

Table 5. The composition of Nd electrodeposits analyzed by EDX.

3.5. Electrodeposition

Considering the above fundamental electrochemical behavior of Nd(III), the electrodeposition of Nd(0) was carried out, and the condition was listed in **Table 4**. The electrodeposition was smoothly performed on the high anodic current efficiency. The current slowly decreased to the limiting current during electrodeposition. After the electrodeposition, the blackish electrodeposits were obtained on the Cu substrate. The electrodeposits observed by SEM had a granular morphology with a nonuniform size distribution. This morphology is considered to be explained from the fact that the initial stage of nucleation and growth occurred according to the progressive nucleation model [15]. The quantitative analysis using EDX for the electrodeposits obtained from the electrodeposition at −3.20 V versus Fc/Fc⁺ is summarized in **Table 5**. The results indicated that the electrodeposits on Cu substrate comprised mainly Nd component. However, a small amount of O component was also included in the electrodeposits, suggesting that the oxidizing Nd metal with O atoms would occur. In order to investigate the chemical bond state of Nd, XPS analysis with Al-Kα was carried out on the electrodeposits. The metallic and oxide components for Nd correspond to the binding energies of Nd3d$_{5/2}$ at 980.5–981.0 eV and 981.7–982.3 eV, respectively, in the case of monochromated Al-Kα line [41]. The Nd3d$_{5/2}$ spectra for the middle layer and top surface of electrodeposits are shown in **Figure 7**. For an in-depth analysis of the middle layer, the oxide layer of the electrodeposits was perfectly removed with an Ar ion beam, that is, (a) 0.42 μm under the electrodeposits. The peak maximum in the Nd3d$_{5/2}$ spectrum acquired for the layers below 0.42 μm was at 980.77 eV. Hence, the electrodeposits obtained through electrodeposition using [P$_{2225}$][TFSA] with M(TFSA)$_3$ were identified as Nd metal and partial oxide mixtures. This result indicated that metallic Nd would have been electrodeposited on the Cu substrate and subsequently oxidized by O in the electrolyte, that is, residual water or dissolved oxygen. The XRD profile of the electrodeposits is shown in **Figure 8** with the profile from Ref. [42] for Nd metal. The position of 2θ of the electrodeposits was nearly identical to that of Nd metal. Therefore, the electrodeposits were identified to be crystalline Nd metal.

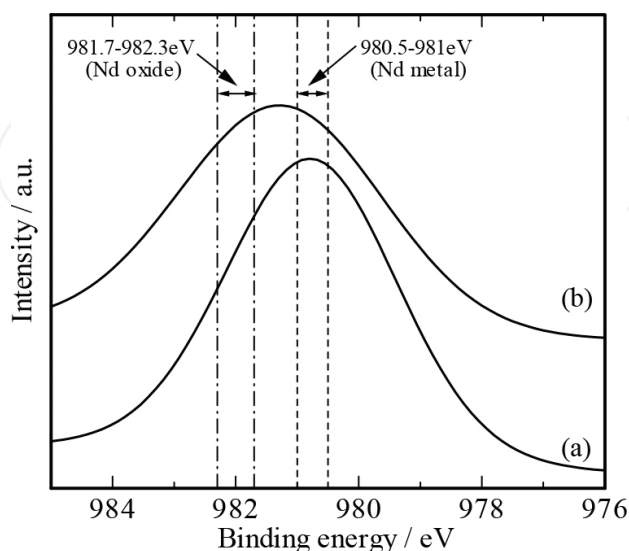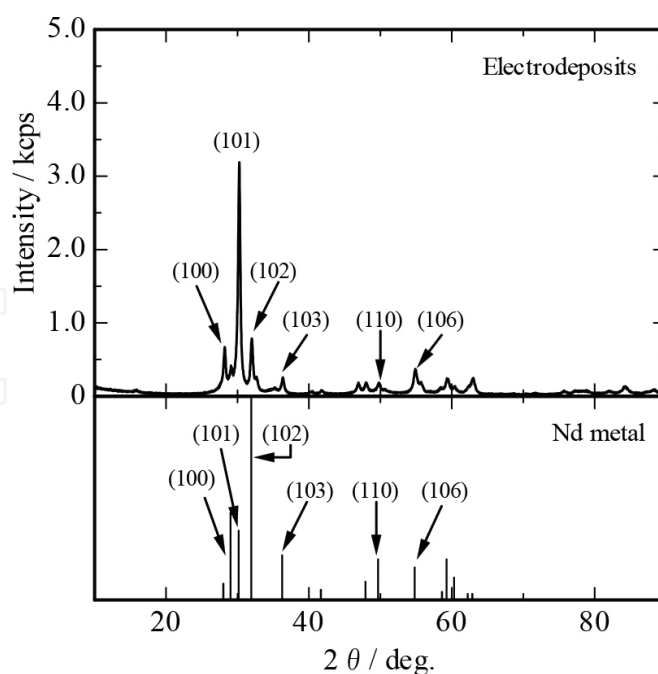**Figure 7.** XPS spectra for Nd3d$_{5/2}$ region of electrodeposits (a) middle layer at ⁻0.42 μm, (b) top surface.

Figure 8. XRD profile of the Nd electrodeposits obtained from [P$_{2225}$][TFSA].

3.6. Material flow of VCM recycling

As described earlier, it is worthwhile to evaluate the material flow from a series of processes such as pretreatment, hydrometallurgy, and electrodeposition using [P$_{2225}$][TFSA] melts. The whole material flow is shown in **Figure 9**, and the recovery target in this material flow was based on the oxidized Nd-Fe-B wastes after the roasting process. As the first step of hydrometallurgy, the selective leaching of RE components (85.7 ± 5.8% Nd and 5.8 ± 0.1% Fe in 66 h) was performed in the leaching process. Then, the deironization treatment was carried out using precipitation formation of [Fe(OH)$_x$]$^{3-x}$, and the residual Fe component was perfectly removed in this process. After the deironization process, the M(TFSA)$_n$ salts with high purity were obtained from the evaporation by a spray dryer, and the yield of M(TFSA)$_n$ salts was as high as 91.7%. Scaling up for the vaporization treatment is relatively simple because a large-scale spray dryer can be available through cooperation with an associated company. A series of hydrometallurgy indicates that 78.6% (356.0 g/453.0 g × 100) Nd and 77.9% (10.9 g/14.0 g) Dy can be recovered as purified M(TFSA)$_n$ salts from the initial oxidized Nd-Fe-B powder. After the hydrometallurgical process, M(TFSA)$_n$ salts were available as an electrolytic bath in the electrodeposition process. In terms of material flow, the induced overpotential ($E = -3.20$ V vs. Fc/Fc$^+$) and the cathodic current efficiency ($\varepsilon = 74.6\%$) were determined from the actual electrodeposition results described above. Assuming that the total transported charge is $Q = 7618.2 \times 10^2$ C (100 times at laboratory scale) under proper conditions based on the scaling-up electrolytic bath, 283.2 g of Nd metal can be recovered during the electrodeposition process, and the recovery yield calculated from the starting material (453.0 g Nd) was estimated to be 62.5%. Therefore, the recovery process based on hydrometallurgy and electrodeposition using [P$_{2225}$][TFSA] was applicable for practical Nd-Fe-B wastes. From the economic point of view,

H[TFSA] is currently slightly expensive compared with mineral acids. However, H[TFSA] can be prepared through an ion-exchange reaction of residual components. Studies to further improve the recovery process are now in progress.
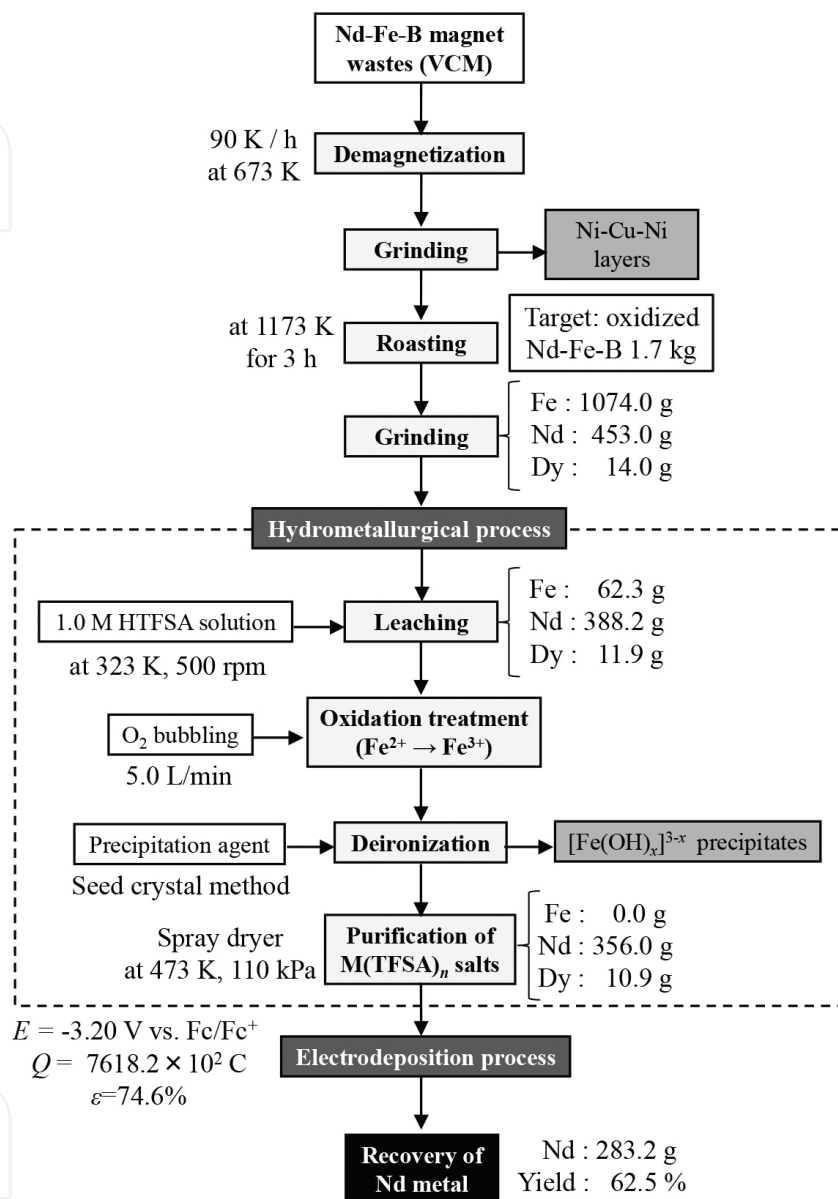

Figure 9. Material flow of hydrometallurgy and electrodeposition using $[P_{2225}][TFSA]$.

4. Conclusion

Hydrometallurgical process based on leaching, deironization, and purification of rare earth (RE) amide salts were carried out at bench scale. In the leaching process using 1.7 kg of oxidized Nd-Fe-B sample and 14.2 L of an aqueous solution of 1,1,1-trifluoro-*N*-[(trifluoromethyl)

sulfonyl]methanesulfonamide ($HN(SO_2CF_3)_2$, H[TFSA]), The leaching percentage of Nd and Fe for 66h in the H[TFSA] solution were 85.7±5.8% and 5.8±0.1%, respectively. Moreover, the oxidized Nd-Fe-B sample applied as a precipitation agent in the deironization process, and >99.9% Fe component was successfully separated from RE components. Finally, 3.57 kg of purified amide salts ($M(TFSA)_3$, M = Pr, Nd, Dy, B, Al, and trace elements) were recovered through the evaporation process using an improved spray dryer and the percentage of RE components for amide salts was 96.81%.

The cyclic voltammetry (CV) with electrochemical quartz crystal microbalance (EQCM) was applied at elevated temperatures in this study. CV/EQCM measurements for the investigation of the reduction behavior related to Nd(III) in triethyl-pentyl-phosphonium bis(trifluoromethyl-sulfonyl)amide ([P_{2225}][TFSA]) were conducted at 373 K. At the potential of −2.79 V, the objective electrodeposition, Nd(III)/Nd(0) was confirmed because a clear cathodic peak was observed and the apparent molar mass, M_{app} was calculated to be 46.8 g mol^{-1}, and this value was consistent with the theoretical value for Nd(III)/Nd(0), 48.1 g mol^{-1}. At more negative potential than −2.79 V, the mass and $\eta\rho$ increased with the comparatively low values of M_{app} for 0.05 M Nd(III) in [P_{2225}][TFSA]. This behavior indicated that the cathodic decomposition reaction of IL occurred on the electrode surface. Moreover, from the controlled potential electrolysis with EQCM (CPE/EQCM) measurements at −3.20 V versus Fc/Fc$^+$ in the solutions of 0.05 and 0.10 M Nd(III) in [P_{2225}][TFSA] at 373 K, the electrodeposits of Nd(0) metal were confirmed at the initial stage considering the M_{app} values (49.1 and 49.6 g mol^{-1}). The electrodeposition of Nd was carried out under potentiostatic conditions of −3.20 V versus Fc/Fc$^+$ at 373 K. The electrodeposits in the middle layer 0.15 μm below the surface were identified to be Nd metal from the analysis of SEM/EDX, XPS, and XRD. Finally, the material flow of whole process allowed us to conclude that the novel recovery process was effective for practical use.

Acknowledgements

Author details

Masahiko Matsumiya

Address all correspondence to: mmatsumi@ynu.ac.jp

Graduate School of Environment and Information Sciences, Yokohama National University, Hodogaya-ku, Yokohama, Japan

References

[1] K. Binnemans, P. T. Jones, B. Blanpain, T. Van Gerven, Y. X. Yang, A. Walton, M. Buchert, Recycling of rare earths: a critical review, J. Clean. Prod. 51 (2013) 1-22.

[2] C. Tunsu, M. Petranikova, M. Gergoric, C. Ekberg, T. Retegan, Reclaiming rare earth elements from end-of-life products: a review of the perspectives for urban mining using hydrometallurgical unit operations, Hydrometallurgy 156 (2015) 239-258.

[3] K. Murase, K. Machida, G. Adachi, Recovery of rare metals from scrap of rare earth intermetallic material by chemical vapor transport, J. Alloys Compd. 217 (1995) 218-225.

[4] Y. Baba, F. Kubota, N. Kamiya, M. Goto, Selective recovery of dysprosium and neodymium ions by a supported liquid membrane based on ionic liquids, Solvent Extr. Res. Dev., Jpn. 18 (2011) 193-198.

[5] M. Fukumoto, M. Odera, K. Yokoyama, M. Hara, Dissolution of Dy_2O_3 and Nd_2O_3 by electrolysis of fused Na_2SO_4 and the recovery of Dy and Nd, Corros. Eng. 61 (2012) 278-282.

[6] T. Nohira, S. Kobayashi, K. Kondo, K. Yasuda, R. Hagiwara, T. Oishi, H. Konishi, Electrochemical formation of RE-Ni (RE = Pr, Nd, Dy) alloys in molten halides, ECS Trans. 50(11) (2013) 473-482.

[7] J. P. Rabatho, W. Tongamp, Y. Takasaki, K. Haga, A. Shibayama, Recovery of Nd and Dy from rare earth magnetic waste sludge by hydrometallurgy, J. Mater. Cycles Waste Manag. 15 (2013) 171-178.

[8] M. Matsumiya, K. Ishioka, T. Yamada, M. Ishii, S. Kawakami, Recovery of rare earth metals from voice coil motors using bis(trifluoromethylsulfonyl)amide melts by wet separation and electrodeposition, Int. J. Miner. Process. 126 (2014) 62-69.

[9] K. Ishioka, M. Matsumiya, M. Ishii, S. Kawakami, Development of energy-saving recycling process for rare earth metals from voice coil motor by wet separation and electrodeposition using metallic-TFSA melts, Hydrometallurgy 144–145 (2014) 186-194.

[10] C. Hamela, P. Chamelot, P. Taxil, Neodymium(III) cathodic processes in molten fluorides, Electrochim. Acta 49 (2004) 4467-4476.

[11] E. Stefanidaki, C. Hasiotis, C. Kontoyannis, Electrodeposition of neodymium from LiF–NdF_3–Nd_2O_3 melts, Electrochim. Acta 46 (2001) 2665-2670.

[12] H. Matsumoto, H. Sakaebe, K. Tatsumi, Preparation of room temperature ionic liquids based on aliphatic onium cations and asymmetric amide anions and their electrochemical properties as a lithium battery electrolyte, J. Power Sources 146 (2005) 45-50.

[13] S. Legeai, S. Diliberto, N. Stein, C. Boulanger, J. Estager, N. Papaiconomou, M. Draye, Room-temperature ionic liquid for lanthanum electrodeposition, Electrochem. Commun. 10 (2008) 1661-1664.

[14]   M. Yamagata, Y. Katayama, Y. Miura, Electrochemical behavior of samarium, europium, and ytterbium in hydrophobic room-temperature molten salt systems, J. Electrochem. Soc. 153 (2006) E5-E9.

[15]   M. Matsumiya, Application of Ionic Liquids on Rare Earth Green Separation and Utilization, Springer (2016) 117-153.

[16]   H. Kondo, M. Matsumiya, K. Tsunashima, S. Kodama, Attempts to the electrodeposition of Nd from ionic liquids at elevated temperatures, Electrochim. Acta, 66 (2012) 313-319.

[17]   M. Ishii, M. Matsumiya, S. Kawakami, ECS Trans. 50(11) (2012) 549-560.

[18]   M. Matsumiya, M. Ishii, K. Kazama, S. Kawakami, Electrochemical analyses of diffusion behaviors and nucleation mechanisms for neodymium complexes in [DEME][TFSA] ionic liquid, Electrochim. Acta 146 (2014) 371-377.

[19]   R. Kazama, M. Matsumiya, N. Tsuda, K. Tsunashima, Electrochim. Acta 113 (2013) 269-279.

[20]   A. Kurachi, M. Matsumiya, K. Tsunashima, S. Kodama, Electrochemical behavior and electrodeposition of dysprosium in ionic liquids based on phosphonium cations, J. Appl. Electrochem. 42 (2012) 961-968.

[21]   M. Matsumiya, Y. Kikuchi, T. Yamada, S. Kawakami, Extraction of rare earth ions by tri-*n*-butylphosphate/phosphonium ionic liquids and the feasibility of recovery by direct electrodeposition, Sep. Purif. Technol. 130 (2014) 91-101.

[22]   Y. Kikuchi, M. Matsumiya, S. Kawakami, Extraction of rare earth ions from Nd-Fe-B magnet wastes with TBP in tricaprylmethylammonium nitrate, Solvent Extr. Res. Dev., Jpn. 21(2) (2014) 137-145.

[23]   S. Murakami, M. Matsumiya, T. Yamada, K. Tsunashima, Solvent Extr. Ion Exch. 34(2) (2016) 172-187.

[24]   G. Z. Sauerbrey, Verwendung von schwingquarzen zur wägung dünner schichten und zur mikrowägung, Z. Phys. 155 (1959) 206-222.

[25]   A. Ispas, B. Adolphi, A. Bund, F. Endres, On the electrodeposition of tantalum from three different ionic liquids with the bis(trifluoromethyl sulfonyl) amide anion, Phys. Chem. Chem. Phys. 12 (2010) 1793-1803.

[26]   N. Serizawa, Y. Katayama, T. Miura, EQCM measurement of Ag(I)/Ag reaction in an amide-type room-temperature ionic liquid, J. Electrochem. Soc. 156(11) (2009) D503-D507.

[27]   N. Serizawa, S. Seki, K. Takei, H. Miyashiro, K. Yoshida, K. Ueno, N. Tachikawa, K. Dokko, Y. Katayama, M. Watanabe, T. Miura, EQCM measurement of deposition and dissolution of lithium in Glyme-Li salt molten complex, J. Electrochem. Soc. 160(9) (2013) A1529-A1533.

[28] F. Endres, S. Z. E. Abedin, A. Y. Saad, E. M. Moustafa, N. Borissenko, W. E. Price, G. G. Wallace, D. R. MacFarlane, P. J. Newman, A. Bund, On the electrodeposition of titanium in ionic liquids, Phys. Chem. Chem. Phys. 10 (2008) 2189-2199.

[29] E. M. Moustafa, S. Z. E. Abedin, A. Shkurankov, E. Zschippang, A. Y. Saad, A. Bund, F. Endres, Electrodeposition of Al in 1-butyl-1-methylpyrrolidinium bis(trifluoromethylsulfonyl)amide and 1-ethyl-3-methylimidazolium bis(trifluorome-thylsulfonyl)amide ionic liquids: in situ STM and EQCM studies, J. Phys. Chem. B 111 (2007) 4693-4704.

[30] A. P. Abbott, A. Nandhra, S. Postlethwaite, E. L. Smith, and K. S. Ryder, Electroless deposition of metallic silver from a choline chloride-based ionic liquid: a study using acoustic impedance spectroscopy, SEM and atomic force microscopy, Phys. Chem. Chem. Phys. 9 (2007) 3735-3743.

[31] H. Muramatsu, A. Egawa, T. Ataka, Reliability of correlation between mass change and resonant frequency change for a viscoelastic-film-coated quartz crystal, J. Electroanal. Chem. 388 (1995) 89-92.

[32] K. Naoi, Y. Oura, M. Maeda, S. Nakamura, Electrochemistry of surfactant-doped polypyrrole film(I): formation of columnar structure by electropolymerization, J. Electrochem. Soc. 142(2) (1995) 417-422.

[33] K. K. Kanazawa, J. G. Gordon II, Frequency of a quartz microbalance in contact with liquid, Anal. Chem. 57 (1985) 1770-1771.

[34] A. Ispas, M. Pölleth, H. T. B. Khanh, A. Bund, J. Janek, Electrochemical deposition of silver from 1-ethyl-3-methylimidazolium trifluoromethanesulfonate, Electrochim. Acta 56 (2011) 10332-10339.

[35] N. Sasaya, M. Matsumiya, S. Murakami, K. Nishihata, K. Tsunashima, Investigation into applicability of EQCM methods at elevated temperature for ionic liquids, Electro-chim. Acta 194 (2016) 304-309.

[36] J. Xu, P. Che, Y. Ma, More sensitive way to determine iron using an iron(II)-1,10-phenanthroline complex and capillary electrophoresis, J. Chromatogr. A 749 (1996) 287-294.

[37] T. Hirokawa, K. Nishimoto, F. Nishiyama, Isotachophoretic separation of Fe(II) and Fe(III) by using 1,10-phenanthroline as a complex-forming agent, J. Chromatogr. A 723 (1996) 389-394.

[38] H. Muramatsu, E. Tamiya, I. Karube, Computation of equivalent circuit parameters of quartz crystals in contact with liquids and study of liquid properties, Anal. Chem. 60 (1988) 2142-2146.

[39] A. Bund, G. Schwitzgebel, Investigations on metal depositions and dissolutions with an improved EQCMB based on quartz crystal impedance, Electrochim. Acta 45 (2000) 3703-3710.

[40]   K. Naoi, M. Mori, Y. Shinagawa, Study of deposition and dissolution processes of lithium in carbonate based solutions by means of the quartz crystal microbalance, J. Electrochem. Soc. 143(8) (1996) 2517-2522.

[41]   J. F. Moulder, W. F. Stickle, P. E. Sobol, K. D. Bomben, Handbook of X-ray Photoelectron Spectroscopy, Perkin-Elmer Corp., Eden Prairie, MN (1992).

[42]   G. C. Che, J. Liang, Y. Yi, Crystal structure of X-ray diffraction properties, J. Metall. 22 (1986) B206-B211.